Available online at www.sciencedirect.com

ScienceDirect

IFAC PapersOnline CONFERENCE PAPER ARCHIVE

IFAC PapersOnLine 52-16 (2019) 192–197

Path following control for articulated intervention-AUVs using geometric control of reduced attitude ⋆

M. Wrzos-Kaminska * **K. Y. Pettersen** * **J. T. Gravdahl** *

* *Centre for Autonomous Marine Operations and Systems, Department of Engineering Cybernetics, Norwegian University of Science and Technology (NTNU), Trondheim, Norway (e-mail: Marianna.Wrzos-Kaminska@ntnu.no, Kristin.Y.Pettersen@ntnu.no, Jan.Tommy.Gravdahl@ntnu.no).*

Abstract: An articulated intervention autonomous underwater vehicle (AIAUV) consists of the jointed body of a snake robot equipped with thrusters for hovering and faster propulsion. The slender, articulated body can be used as a floating manipulator arm for subsea intervention. In order to extend the reach and operation time of the AIAUV, energy-efficient methods for long-distance travel are needed. This paper proposes a path-following control method for AIAUVs moving in 3D which reduces the use of thrusters by using them only for forward propulsion. The direction of travel is controlled by curving the body using its joints. As a first step, a control law for tracking of a reduced attitude is developed for a general system with two control torques, and shown to give asymptotic tracking of a time-varying reference reduced attitude. This control law is then used indirectly to provide references for the joint angles of an AIAUV, in order to control its pointing direction. By combining this with a line-of-sight (LOS) guidance law, a method for following straight paths is obtained. Simulation studies show that the method succeeds in making an AIAUV converge to and follow the desired path.

Keywords: Articulated Intervention Autonomous Underwater Vehicle, Path Following, Attitude Control, Autonomous Underwater Vehicle, Underwater Swimming Manipulator

1. INTRODUCTION

The increasing exploration and utilization of our oceans require a wide range of tasks to be performed underwater, from surveying and mapping, to construction and subsequent maintenance of underwater structures. Surveying to an increasing degree performed by autonomous underwater vehicles (AUVs). These typically have a slender torpedo shape for speed and efficiency. However, they are not equipped to perform intervention tasks, nor are they able to hover. In contrast, tasks requiring intervention are largely performed using remotely operated vehicles (ROVs) tethered to a mother vessel. A typical work-class ROV consists of a large body with an arm attached, and is built for stability, not speed and range.

The articulated intervention-AUV (AIAUV) is a cross between an underwater snake robot (USR) and a torpedo-shaped AUV. It possesses the articulated, jointed body of the USR, combined with several thrusters, both longitudinal thrusters for faster propulsion, and tunnel thrusters to provide the ability of station-keeping. The articulated body can also be used as a free-floating manipulator arm, i.e. an underwater swimming manipulator (USM). With its slender, jointed body the AIAUV has superior access to narrow and confined spaces, making it well-suited for inspection, maintenance and light intervention tasks at subsea structures (Sverdrup-Thygeson et al., 2018).

When travelling or surveying, the AIAUV can be straightened into a torpedo-like shape. In order to extend operation time and reach, energy-efficient methods of travel are crucial. Previous work considering this transport mode for the AIAUV use tunnel thrusters either as the sole means of turning (Borlaug et al., 2018a), or in combination with curving the body towards the path to be followed (Sverdrup-Thygeson et al., 2016). In Sans-Muntadas et al. (2017), an AIAUV possessing only longitudinal tail thrusters was used to experimentally demonstrate docking along a spiral path, using its joints for direction control. Turning by curving the body not only reduces the use of thrusters, but is also more hydrodynamically efficient.

The idea of turning by curving the body traces back to biological swimmers, such as eels or swimming snakes, and has been successfully applied to USRs. By using a guidance law to determine the curve, a USR was made to swim onto a straight path in Kelasidi et al. (2016), and similarly following curved paths has been considered by Lapierre and Jouvencel (2005), and Kohl et al. (2016). In Guo (2006), waypoint tracking is achieved in a similar way for a fish-like AUV by curving a two-segment tail attached to its body. Notably, all of these works consider only planar motion. AIAUV motion in three dimensions is considered in Borlaug et al. (2018b), where thrusters are used to

⋆ This research was funded by the Research Council of Norway through the Centres of Excellence funding scheme, project No. 223254 NTNU AMOS.

10.1016/j.ifacol.2019.11.777

track a desired position and orientation of the backmost link of the body, while the joints are given trajectories independently.

A guidance principle frequently used in path following for AUVs is the line-of-sight (LOS) principle (Fossen, 2011), which aims the vehicle towards a point further ahead along the path. In 3D, this provides only a pointing direction, not a full attitude reference. Many AUVs are passively stabilised in roll, in which case the control problem can be simplified from a total of 6 degrees of freedom (DOF) to 5 by disregarding it, as in Caharija et al. (2012), or a reference for the full attitude can be found (Woolsey, 2006). However, due to the AIAUV's dual use as both a vehicle and a free-floating manipulator, it may not be desirable to heavily stabilise it, because this could impede its dexterity as a manipulator. The AIAUV thus requires control of its pointing direction, or reduced attitude, which does not assume anything about roll.

Reduced attitude stabilisation has been addressed by e.g. Chaturvedi et al. (2011), while in Pong and Miller (2015); Ramp and Papadopoulos (2015), the problem of reduced attitude tracking is addressed for spacecraft fully actuated in attitude. Reduced attitude stabilisation using only two control torques has been done by Bullo et al. (1995), as well as tracking, using accelerations along the surface of the sphere as inputs.

In this paper, a control law for tracking of a reduced attitude is proposed for a general system with only two control torques, and the control law is shown to asymptotically stabilise the tracking errors. The control law is used as a basis for controlling the pointing direction of an AIAUV by means of its joints. Combined with a LOS guidance law, this results in a path-following method for AIAUVs moving in 3D. This method has been developed with the aim of consuming less energy than previous methods like those of Sverdrup-Thygeson et al. (2016) or Borlaug et al. (2018a), by avoiding the additional use of thrusters for turning. The method is verified through simulations.

The rest of this paper is structured as follows: in Section 2 the reduced attitude tracking control for a general system is presented and analysed. Section 3 presents the path-following and pointing direction control methods for AIAUVs, and simulation results are shown in Section 4. Finally, conclusions are given in Section 5.

2. TRACKING OF A REDUCED ATTITUDE

In this section, a control law solving the problem of tracking a reduced attitude, or pointing direction, using only two control torques is proposed, and we show that it gives asymptotic tracking of a time-varying reference.

2.1 Problem dynamics and kinematics

The attitude dynamics of a rigid body equipped with two control torques can be written as

$$J\dot{\boldsymbol{\omega}}^b = \boldsymbol{m} + H\boldsymbol{u} \tag{1}$$

where $\boldsymbol{\omega}^b \in \mathbb{R}^3$ is the angular velocity of the rigid body given in its body-fixed frame, $J = J^\top > 0$ is the 3×3 inertia matrix, $\boldsymbol{u} \in \mathbb{R}^2$ is the control input, and $\boldsymbol{m} \in \mathbb{R}^3$ represents all other moments acting on the system, which are assumed to be known. The matrix $H = [\boldsymbol{e}_2\ \boldsymbol{e}_3] \in \mathbb{R}^{3\times 2}$ maps the two control torques to the actuated axes $\boldsymbol{e}_2$, $\boldsymbol{e}_3$ of the body-fixed frame.

Assumption 1. The inertia matrix J is assumed to have the block-diagonal structure

$$J = \begin{bmatrix} J_{11} & 0 \\ 0 & J_{22} \end{bmatrix} \tag{2}$$

where $J_{11} \in \mathbb{R}$, and $J_{22} \in \mathbb{R}^{2\times 2}$. Since J is a positive definite matrix, J_{22} is also positive definite (Bernstein, 2009).

Remark 1. Assumption 1 can be fulfilled either by aligning the body-frame axes with the principal axes of inertia of the rigid body, or by ensuring reflection symmetry through either the yz-plane, or both the xy- and xz-plane of the body frame (Fossen, 2011).

The reference pointing direction is given in the inertial frame I as a function $\boldsymbol{x}^I_{\text{ref}}(t)$ such that $\|\boldsymbol{x}^I_{\text{ref}}(t)\| = 1\,\forall\, t$. Its angular velocity expressed in the body frame is

$$\boldsymbol{\omega}^b_{\text{ref}} = R^b_I\left(\boldsymbol{x}^I_{\text{ref}} \times \dot{\boldsymbol{x}}^I_{\text{ref}}\right) = \boldsymbol{x}^b_{\text{ref}} \times \left(R^b_I \dot{\boldsymbol{x}}^I_{\text{ref}}\right) \tag{3}$$

where $R^b_I = R^{I\top}_b$, and R^I_b describes the full orientation of the body frame b.

As in Pong and Miller (2015), the control law will be realised in the body frame, in which the directions of the control inputs are fixed. The control objective is to align the body-frame representation $\boldsymbol{x}^b_{\text{ref}} = R^b_I \boldsymbol{x}^I_{\text{ref}}$ of the reference with the unactuated axis $\boldsymbol{e}_1$ of the body frame. The shortest distance between the two vectors along the surface of the unit sphere $\mathbb{S}^2$ is equal to the angle $\tilde{\phi}$ between them, given as

$$\tilde{\phi} = \arccos(\boldsymbol{e}_1^\top \boldsymbol{x}^b_{\text{ref}})\ . \tag{4}$$

Let $\tilde{R}$ be the rotation matrix rotating $\boldsymbol{x}^b_{\text{ref}}$ to $\boldsymbol{e}_1$, such that $\tilde{R}\boldsymbol{x}^b_{\text{ref}} = \boldsymbol{e}_1$. The rotation described by $\tilde{R}$ is a rotation about the axis parallel to $\boldsymbol{x}^b_{\text{ref}} \times \boldsymbol{e}_1$ by an angle $\tilde{\phi}$. Using the fact that $\|\boldsymbol{x}^b_{\text{ref}} \times \boldsymbol{e}_1\| = \sin\tilde{\phi}$, $\tilde{R}$ can be expressed as

$$\tilde{R} = I_3 + S\left(\boldsymbol{x}^b_{\text{ref}} \times \boldsymbol{e}_1\right) + \left(\frac{1-\cos\tilde{\phi}}{\sin^2\tilde{\phi}}\right) S^2\left(\boldsymbol{x}^b_{\text{ref}} \times \boldsymbol{e}_1\right) \tag{5}$$

where $S(\boldsymbol{v})\boldsymbol{w} = \boldsymbol{v} \times \boldsymbol{w}$ for $\boldsymbol{v}$, $\boldsymbol{w} \in \mathbb{R}^3$. Since $\tilde{R}$ can also be interpreted as describing the orientation of a frame obtained by rotating the body frame by $\tilde{R}$, its derivative is $\dot{\tilde{R}} = \tilde{R}S(\boldsymbol{\omega}^b - \boldsymbol{\omega}^b_{\text{ref}})$ (Egeland and Gravdahl, 2002). Consequently,

$$\dot{\boldsymbol{x}}^b_{\text{ref}} = \dot{\tilde{R}}^\top \boldsymbol{e}_1 = -(\boldsymbol{\omega}^b - \boldsymbol{\omega}^b_{\text{ref}}) \times \boldsymbol{x}^b_{\text{ref}}\ . \tag{6}$$

This allows to express the dynamics of the error $\tilde{\phi}$ as

$$\begin{aligned}\dot{\tilde{\phi}} &= \frac{-1}{\sqrt{1-\left(\boldsymbol{e}_1^\top \boldsymbol{x}^b_{\text{ref}}\right)^2}} \boldsymbol{e}_1^\top \dot{\boldsymbol{x}}^b_{\text{ref}} = \frac{1}{\sin\tilde{\phi}} \boldsymbol{e}_1^\top \left(\left(\boldsymbol{\omega}^b - \boldsymbol{\omega}^b_{\text{ref}}\right) \times \boldsymbol{x}^b_{\text{ref}}\right) \\ &= \frac{1}{\sin\tilde{\phi}} \left(\boldsymbol{\omega}^b - \boldsymbol{\omega}^b_{\text{ref}}\right)^\top \left(\boldsymbol{x}^b_{\text{ref}} \times \boldsymbol{e}_1\right)\end{aligned} \tag{7}$$

where the equivalence of the scalar triple product has been used. The difference $\boldsymbol{\omega}^b - \boldsymbol{\omega}^b_{\text{ref}}$ between the angular velocities is unsuited to use for feedback, as it cannot be realised by the available control inputs. This problem is addressed by Bullo et al. (1995), where the matrix $\tilde{R}$ is used to rotate the angular velocity of the reference, which lies in a plane tangential to the unit sphere at the point $\boldsymbol{x}^b_{\text{ref}}$, into the tangent plane at $\boldsymbol{e}_1$, which is also the plane spanned by the two unactuated axes. This allows us to formulate an angular velocity error $\tilde{\boldsymbol{\omega}}^b \in \mathbb{R}^2$ which can be fully realised by the available control inputs, given as

$$\tilde{\boldsymbol{\omega}}^b = H^\top(\boldsymbol{\omega}^b - \tilde{R}\boldsymbol{\omega}^b_{\text{ref}}). \tag{8}$$

Multiplication by $H^\top$ disregards only the angular velocity of the body about the first axis of the body frame, which does not influence its pointing direction.

The control objective is thus to stabilise the errors $(\tilde{\phi}, \tilde{\boldsymbol{\omega}}^b)$ to zero, in which case $\boldsymbol{e}_1$ is aligned with the reference and has no angular velocity relative to the reference except rotation about itself. Hence tracking is achieved when the errors $(\tilde{\phi}, \tilde{\boldsymbol{\omega}}^b)$ are zero.

2.2 Control law and closed-loop error dynamics

To achieve the control objective, we propose the following control law:

$$\boldsymbol{u} = -k_P \tilde{\phi} H^\top \boldsymbol{n} - k_D \tilde{\boldsymbol{\omega}}^b + H^\top \Big(J \tilde{R} R_I^b \big(\boldsymbol{x}_{\text{ref}}^I \times \ddot{\boldsymbol{x}}_{\text{ref}}^I \big) - \boldsymbol{m} \Big) \quad (9)$$

where $\boldsymbol{n} = \frac{\boldsymbol{x}_{\text{ref}}^b \times \boldsymbol{e}_1}{\| \boldsymbol{x}_{\text{ref}}^b \times \boldsymbol{e}_1 \|}$. The control law (9) is inspired by the works of Bullo et al. (1995) and Pong and Miller (2015), but unlike the tracking law proposed by Bullo et al. (1995), the inputs are torques, requiring the inertia of the system to be taken into account, and unlike in Pong and Miller (2015), the system (1) considered here is underactuated. The term $\tilde{\phi}\boldsymbol{n}$ and matrix $\tilde{R}$ are not defined at $\tilde{\phi} = 0 \vee \pi$. At these points, we define $\tilde{\phi}\boldsymbol{n}$ to be zero, and $\tilde{R} = I_3$.

The dynamics of the angular velocity error $\tilde{\boldsymbol{\omega}}^b$ are

$$\begin{aligned} \dot{\tilde{\boldsymbol{\omega}}}^b &= H^\top \Big(\dot{\boldsymbol{\omega}}^b - \dot{\tilde{R}} \boldsymbol{\omega}_{\text{ref}}^b - \tilde{R} \dot{\boldsymbol{\omega}}_{\text{ref}}^b \Big) \\ &= H^\top \Big(J^{-1} \left(\boldsymbol{m} + H\boldsymbol{u} \right) - \tilde{R} \left(\left(\boldsymbol{\omega}^b - \boldsymbol{\omega}_{\text{ref}}^b \right) \times \boldsymbol{\omega}_{\text{ref}}^b \right) \\ &\quad - \tilde{R} \left(-\boldsymbol{\omega}^b \times \boldsymbol{\omega}_{\text{ref}}^b + R_I^b \left(\boldsymbol{x}_{\text{ref}}^I \times \ddot{\boldsymbol{x}}_{\text{ref}}^I \right) \right) \Big) \\ &= H^\top \Big(J^{-1} \left(\boldsymbol{m} + H\boldsymbol{u} \right) - \tilde{R} R_I^b \left(\boldsymbol{x}_{\text{ref}}^I \times \ddot{\boldsymbol{x}}_{\text{ref}}^I \right) \Big) \end{aligned} \quad (10)$$

For a vector $\boldsymbol{v} \perp \boldsymbol{e}_1$ it holds that $HH^\top \boldsymbol{v} = \boldsymbol{v}$. Furthermore, the block-diagonal structure of J results in $J^{-1} H H^\top J = H H^\top$. After rotation by $\tilde{R}$, the angular acceleration term $R_I^b (\boldsymbol{x}_{\text{ref}}^I \times \ddot{\boldsymbol{x}}_{\text{ref}}^I)$ is perpendicular to $\boldsymbol{e}_1$, and can therefore be fully cancelled by the chosen input. Inserting the control law (9) for $\boldsymbol{u}$, and using the fact that $H^\top J^{-1} H = J_{22}^{-1}$, gives

$$\begin{aligned} \dot{\tilde{\boldsymbol{\omega}}}^b = J_{22}^{-1} \Bigg(-k_P \frac{\tilde{\phi}}{\sin \tilde{\phi}} H^\top \left(\boldsymbol{x}_{\text{ref}}^b \times \boldsymbol{e}_1 \right) - k_D \tilde{\boldsymbol{\omega}}^b \Bigg) \\ + H^\top J^{-1} (I_3 - H H^\top) \boldsymbol{m} \end{aligned} \quad (11)$$

The block-diagonal structure of J, and consequently J^{-1}, means that the term $J^{-1}(I_3 - HH^\top)\boldsymbol{m}$ is parallel to $\boldsymbol{e}_1$, and therefore disappears upon multiplication with $H^\top$. In other words, while the torque $\boldsymbol{m}$ is only partially cancelled by the control input, what is not cancelled is only the torque about the unactuated axis, which does not influence its pointing direction. The closed-loop error dynamics of the angular velocity are then

$$\dot{\tilde{\boldsymbol{\omega}}}^b = -k_P \frac{\tilde{\phi}}{\sin \tilde{\phi}} J_{22}^{-1} H^\top \left(\boldsymbol{x}_{\text{ref}}^b \times \boldsymbol{e}_1 \right) - k_D J_{22}^{-1} \tilde{\boldsymbol{\omega}}^b \ . \quad (12)$$

Theorem 1. For a system with dynamics (1) and subject to Assumption 1, the control law (9) asymptotically stabilises the origin $(\tilde{\phi}, \tilde{\boldsymbol{\omega}}^b)$ of the closed-loop system dynamics (7), (12) from any initial conditions $(\tilde{\phi}(0), \tilde{\boldsymbol{\omega}}^b(0))$ such that

$$\pi^2 > \tilde{\phi}(0)^2 + \frac{1}{k_P} \tilde{\boldsymbol{\omega}}^b(0)^\top J_{22} \tilde{\boldsymbol{\omega}}^b(0) \ . \quad (13)$$

2.3 Stability

In this section we present the proof of Theorem 1.

Consider the domain $[0, \pi) \times \mathbb{R}^2$, denoted D, and a Lyapunov function candidate $V(\tilde{\phi}, \tilde{\boldsymbol{\omega}}^b) : D \to \mathbb{R}$ chosen as

$$V = \frac{k_P}{2} \tilde{\phi}^2 + \frac{1}{2} \tilde{\boldsymbol{\omega}}^{b\top} J_{22} \tilde{\boldsymbol{\omega}}^b \ . \quad (14)$$

which is a positive definite, continuously differentiable function on the domain D. Differentation of (14) and inserting the error dynamics (7), (12) gives

$$\begin{aligned} \dot{V} &= k_P \tilde{\phi} \dot{\tilde{\phi}} + \tilde{\boldsymbol{\omega}}^{b\top} J_{22} \dot{\tilde{\boldsymbol{\omega}}}^b \\ &= -k_D \| \tilde{\boldsymbol{\omega}}^b \|^2 + k_P \frac{\tilde{\phi}}{\sin \tilde{\phi}} \Big(\left(\boldsymbol{\omega}^b - \boldsymbol{\omega}_{\text{ref}}^b \right)^\top \left(\boldsymbol{x}_{\text{ref}}^b \times \boldsymbol{e}_1 \right) \\ &\quad - \left(\boldsymbol{\omega}^b - \tilde{R} \boldsymbol{\omega}_{\text{ref}}^b \right)^\top H H^\top \left(\boldsymbol{x}_{\text{ref}}^b \times \boldsymbol{e}_1 \right) \Big) \\ &= -k_D \| \tilde{\boldsymbol{\omega}}^b \|^2 + k_P \frac{\tilde{\phi}}{\sin \tilde{\phi}} \Big(\left(\boldsymbol{\omega}^b - \boldsymbol{\omega}_{\text{ref}}^b \right)^\top \left(\boldsymbol{x}_{\text{ref}}^b \times \boldsymbol{e}_1 \right) \\ &\quad - \boldsymbol{\omega}^{b\top} \left(\boldsymbol{x}_{\text{ref}}^b \times \boldsymbol{e}_1 \right) + \boldsymbol{\omega}_{\text{ref}}^{b\top} \tilde{R}^\top \left(\boldsymbol{x}_{\text{ref}}^b \times \boldsymbol{e}_1 \right) \Big) \ . \end{aligned} \quad (15)$$

Since $\tilde{R}^\top$ describes a rotation about an axis parallel to $\boldsymbol{x}_{\text{ref}}^b \times \boldsymbol{e}_1$, this vector is not changed by premultiplication with $\tilde{R}$, which gives

$$\dot{V} = -k_D \| \tilde{\boldsymbol{\omega}}^b \|^2 \ . \quad (16)$$

The derivative of V can remain zero only when $\tilde{\boldsymbol{\omega}}^b = 0$. In this case, the dynamics (12) of $\tilde{\boldsymbol{\omega}}^b$ simplifies to

$$\dot{\tilde{\boldsymbol{\omega}}}^b = -k_P \phi J_{22}^{-1} H^\top \boldsymbol{n} \quad (17)$$

By design of the input $\boldsymbol{u}$, the term $\phi\boldsymbol{n}$ is equal to 0 when $\tilde{\phi} = 0 \vee \pi$, the second of which is not in the considered domain D. Hence the origin is the only invariant subset of the set $\{\tilde{\phi}, \tilde{\boldsymbol{\omega}}^b \in D \,|\, \dot{V} = 0\}$, and by LaSalle's theorem (Khalil, 2002), it is asymptotically stable. It can further be shown that the set of states which fulfil (13) is a positively invariant subset of the domain D, so that every trajectory starting in this set will converge to the origin.

3. PATH FOLLOWING

In this section, the attitude control law developed in Section 2 is used to provide not control torques, but references for the joints of the AIAUV. This way, the pointing direction of the AIAUV is controlled indirectly by curving its body. This is combined with a guidance law to achieve path following of straight paths in 3D space.

3.1 Control objective

The task to be solved is for the front of the head link, where an end-effector or camera typically is mounted, to converge towards and follow a straight path in a 3-dimensional space. Without loss of generality, the path is chosen to be parallel to the x-axis of an inertial reference frame. The control objective of following the path is then equivalent to driving the y- and z-positions, p_y, p_z, of the end-effector in the inertial frame to 0, while maintaining a desired constant forward velocity u_d, which can be formalised as

$$\lim_{t \to \infty} p_y = 0, \quad \lim_{t \to \infty} p_z = 0, \quad \lim_{t \to \infty} u = u_d \quad (18)$$

where u denotes the surge velocity of the end-effector.

3.2 Vehicle model

The AIAUV can be modelled as n cylindrical links connected by $n-1$ 1-DOF joints, numbered $i = 1, ..., n-1$

from tail to head. Each link has a reference frame attached, with x-axis pointing forward along the link, and z-axis up. The AIAUV is equipped with m thrusters. Viewing the tail link as the base of a manipulator, the AIAUV can be modelled as an underwater vehicle-manipulator system with dynamics given by Antonelli (2018) as

$$M(\boldsymbol{q})\dot{\boldsymbol{\zeta}} + C(\boldsymbol{q},\boldsymbol{\zeta})\boldsymbol{\zeta} + D(\boldsymbol{q},\boldsymbol{\zeta})\boldsymbol{\zeta} + \boldsymbol{g}(\boldsymbol{q},\boldsymbol{\eta}) = \boldsymbol{\tau}(\boldsymbol{q}) \quad (19)$$

where $\boldsymbol{q} \in \mathbb{R}^{(n-1)}$ is a vector of joint angles, $\boldsymbol{\eta}$ describes the position and orientation of the base link, and $\boldsymbol{\zeta} = [\boldsymbol{v}^\top \ \boldsymbol{\omega}^\top \ \dot{\boldsymbol{q}}] \in \mathbb{R}^{6+(n-1)}$ is a vector of body-fixed velocities, where $\boldsymbol{v}$ and $\boldsymbol{\omega}$ are the linear and angular velocities of the base link, respectively. The matrix $M(\boldsymbol{q})$ is the inertia matrix, including added mass effects, $C(\boldsymbol{q},\boldsymbol{\zeta})$ is the Coriolis and centripetal matrix, and $D(\boldsymbol{q},\boldsymbol{\zeta})$ is the damping matrix. The hydrostatic restoring forces $\boldsymbol{g}(\boldsymbol{q},\boldsymbol{\eta})$ acting on the base link and joints can be found from the hydrostatic forces acting on each link (From et al., 2014).

Based on Schmidt-Didlaukies et al. (2018), the generalised control input $\boldsymbol{\tau}(\boldsymbol{q})$ can be written as

$$\boldsymbol{\tau}(\boldsymbol{q}) = \begin{bmatrix} B(\boldsymbol{q}) & 0_{6\times(n-1)} \\ & I_{(n-1)} \end{bmatrix} \begin{bmatrix} \boldsymbol{\tau}_{\text{thr}} \\ \boldsymbol{\tau}_q \end{bmatrix} \quad (20)$$

where $B(\boldsymbol{q}) \in \mathbb{R}^{(6+n-1)\times m}$ is the thrust configuration matrix, and the inputs $\boldsymbol{\tau}_{\text{thr}} \in \mathbb{R}^m$ and $\boldsymbol{\tau}_q \in \mathbb{R}^{n-1}$ are thruster forces and joint torques, respectively.

3.3 Guidance

The following guidance law is a vector formulation of the LOS principle. It is obtained by extending the guidance law for surface vessels from Paliotta and Pettersen (2016) to 3D. The desired direction of travel $\boldsymbol{\mu}^I_{\text{ref}}$ is then

$$\boldsymbol{\mu}^I_{\text{ref}} = u_d \boldsymbol{e}_1 - k_e \left[0,\ p_y,\ p_z\right]^\top \quad (21)$$

where u_d is the desired forward velocity, and k_e is a design parameter. The guidance law is illustrated in Fig. 1. The parameter k_e adjusts the convergence rate towards the path. Different weighting of the errors p_y, p_z, achieving different convergence rates, can be obtained by replacing the scalar k_e with a diagonal matrix.

3.4 Joint angle references for direction control

The AIAUVs considered in this paper are assumed to have an equal number of joints actuated about the y- and z-axes of the link frames to which they are attached. As previously discussed, the approach proposed in this paper will use the joints for direction control, by curving the body of the AIAUV to achieve a turning motion. In order to keep the pointing direction of the end-effector steady, it is desirable to use the joints towards the back of the AIAUV more than those in the front, near the end-effector. In Sans-Muntadas et al. (2017), the joint references increase linearly towards the tail. In this paper, we propose an exponential scaling factor for the joint references, inspired by the head-to-tail amplitude ratio of swimming biological eels (Piñeirua et al., 2015).

Let $q_{a,j}$, $j = 1, ..., \frac{n-1}{2}$ denote the jth joint among the joints actuated about axis $a = y, z$, numbered from tail to head. The reference angle $q^*_{a,j}$ is chosen as

$$q^*_{a,j} = e^{-\alpha(j-1)}\text{sat}(q_{a,0}) \quad (22)$$

where $q_{a,0}$ is a base angle common for all joints rotating about the same axis, to be specified later. The sat$(\cdot)$-function is used to saturate the reference at a maximum angle $q_{\max}$ in order to preserve the shape of the curve despite physical joint limitations. The shape of the curve can be adjusted by choice of the parameter $\alpha > 0$. Larger values of α will result in keeping the front of the AIAUV more straight and using primarily the joints towards the back to turn, reminiscent of the tail of a fish or the rudder of a traditional marine vehicle, whereas a lower value of α will result in all joints being used more equally, giving a more uniform curve of the body.

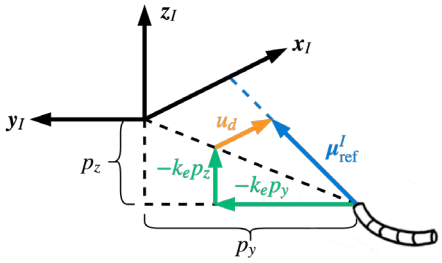

Fig. 1. Illustration of the guidance law (21). The axes of the inertial frame are denoted x_I, y_I, z_I.

Now let $\boldsymbol{q}_0 = [q_{y,0}, q_{z,0}]^\top$ be a vector consisting of the base reference angles for the joints actuated about the y- and z-axes, respectively. Based on the control law (9), these are chosen to be

$$\boldsymbol{q}_0 = -k_P \tilde{\phi} H^\top \boldsymbol{n} - k_D \tilde{\boldsymbol{\omega}}^e + H^\top \tilde{R} R^e_I \left(\boldsymbol{x}^I_{\text{ref}} \times \ddot{\boldsymbol{x}}^I_{\text{ref}}\right) \quad (23)$$

where e denotes the end-effector frame, parallel to the frame of the head link, but placed at its front. The angle $\tilde{\phi}$ is the angle between the end-effector and inertial frame x-axes. The reference pointing direction $\boldsymbol{x}^I_{\text{ref}}$ is the unit vector parallel to $\boldsymbol{\mu}^I_{\text{ref}}$ from the guidance law (21). Since the base angles influence the pointing direction of the AIAUV indirectly, the last term of (23) serves to incorporate some information about the future motion of the reference, but will not necessarily ensure tracking.

As in Section 2, the term $\tilde{\phi}\boldsymbol{n}$ is set to zero when the reference and current pointing direction are parallel. However, the AIAUV can only remain pointing opposite its reference if it is travelling along the path in the opposite direction with straightened joints.

3.5 Velocity and joint control

Joints As in Sverdrup-Thygeson et al. (2016), the joints will be controlled using a PD-controller, but with an additional term compensating for the hydrostatic forces acting on the individual joints. The ith element $\tau_{q,i}$ of the control input $\boldsymbol{\tau}_q$ is set to

$$\tau_{q,i} = -k_{q,P}(q_i - q^*_i) - k_{q,D}\dot{q}_i + \boldsymbol{g}_q \quad (24)$$

where q^*_i denotes the reference for joint i among all joints. The term $\boldsymbol{g}_q$ denotes the part of the generalised hydrostatic force $\boldsymbol{g}(\boldsymbol{\eta},\boldsymbol{q})$ from (20) which influences the joints. In order to avoid differentiating the joint reference (22), the controller (24) effectively treats the reference as a setpoint.

Forward velocity The forward velocity will be controlled using only the longitudinal thrusters of the AIAUV. The ith element $\tau_{\text{thr},i}$ of $\boldsymbol{\tau}_{\text{thr}}$ is set to

$$\tau_{\text{thr},i} = -k_{1,P}(u - u_d) - k_{1,I}\int_0^t u(\tau) - u_d \ \mathrm{d}\tau \quad (25)$$

if thruster i acts in the x-direction of the link frame to which it is attached, and zero otherwise.

Table 1. Link properties

Link no.	Length [m]	Mass [kg]	Thrusters
1	0.62	14.3	None
2, 4, 6, 8	0.104	6.0	None
3	0.584	12.7	2: Z, Y
5	0.726	9.8	3: X, X, Z
7	0.584	12.7	2: Y, Z
9	0.37	7.8	None

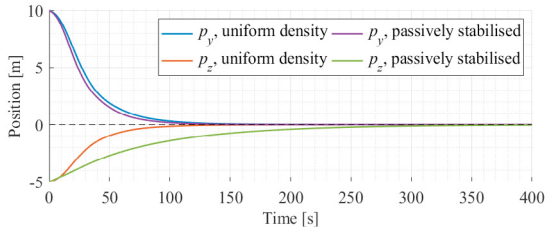

Fig. 2. Cross-track errors

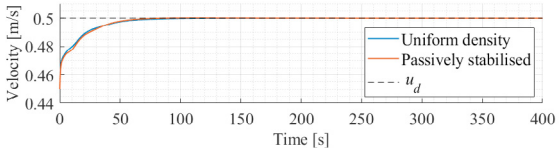

Fig. 3. Surge velocity

4. SIMULATION RESULTS

4.1 Implementation

The simulation model is implemented in MATLAB/Simulink, based on Schmidt-Didlaukies et al. (2018). The model is based on an AIAUV with universal joints, modelled as two consecutive joints with a short link between them. The resulting model has $n = 9$ links with radius 0.085 m, and 8 1-DOF revolute joints. Joints 1, 3, 5, 7 rotate about the z-axis, and joints 2, 4, 6, 8 about the y-axis. The link properties are given in Tab. 1. The vehicle has $m = 7$ thrusters. The notation "2: Z, Y" in Tab. 1 means that the link has two thrusters, acting in the z- and y-direction respectively.

4.2 Simulations

Simulations were performed for two cases, one where each link of the vehicle has uniform density, and one where the links are each passively stabilised in roll. In both cases, the vehicle is neutrally buoyant. The direction of gravity is downwards, parallel to the inertial z-axis.

The reference velocity is $u_d = 0.5$ m/s, and $k_e = \frac{u_d}{10}$. The desired body shape is given by $\alpha = 0.7$. The attitude control gains are $k_P = 2$ and $k_D = 19$ for the AIAUV with uniform density, while $k_D = 12$ in the passively stabilised case, due to the natural hydrostatic damping. Controller parameters were chosen as $k_{q,P} = 30$, $k_{q,D} = 50$, $k_{1,P} = 100$, $k_{1,I} = 5$. The vehicle starts parallel to the path.

The cross-track errors from the simulations are shown in Fig. 2, and surge velocity in Fig. 3. Fig. 4, 5 and 6 show the error angle $\tilde{\phi}$, angular velocity error $\tilde{\boldsymbol{\omega}}^e$ and base angles $q_{y,0}$, $q_{z,0}$, respectively. In addition, Fig. 7 shows the inertial-frame representation $\boldsymbol{x}^I$ of the end-effector x-axis, for the case of uniform density.

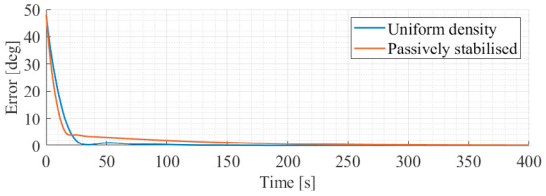

Fig. 4. Error angle $\tilde{\phi}$ between current and reference pointing direction

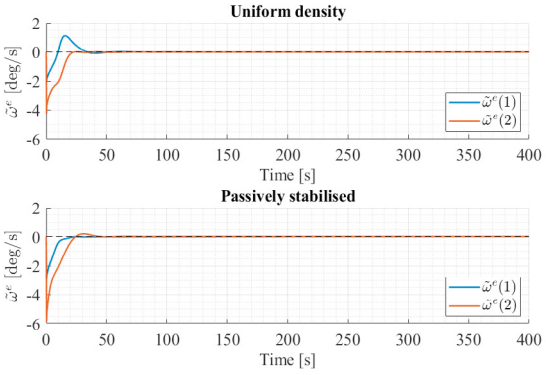

Fig. 5. Angular velocity error $\tilde{\boldsymbol{\omega}}^e$

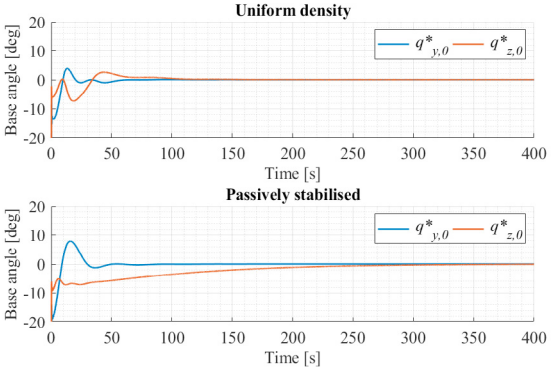

Fig. 6. Base angles for the joint references

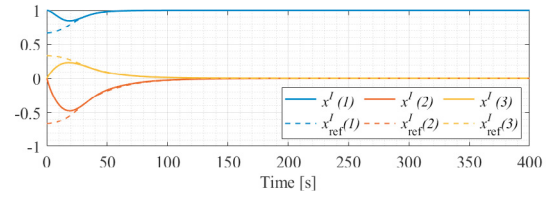

Fig. 7. End-effector and reference pointing direction in the inertial frame, for the vehicle with uniform density.

4.3 Discussion

As can be seen from Fig. 2 and 3, the control objectives (18) are successfully met. Furthermore, Fig. 4 and 5 show that the errors $\tilde{\phi}$ and $\tilde{\boldsymbol{\omega}}^e$ converge to zero, albeit slowly in the passively stabilised case. This is achieved despite the fact that the control law (9) is used only indirectly to provide joint angle references.

In the case of following a straight path, the reference pointing direction converges to a constant. As can be seen from Fig. 7, perfect tracking of the reference direction is not achieved before the reference has converged. The dynamics of the turning motion with joint angles as inputs have

not been derived, and have therefore not been cancelled or otherwise compensated by the proposed method of direction control. Deriving these dynamics would also allow to examine what conditions the system must meet to achieve perfect tracking using joints for direction control.

As previously mentioned, the proposed control method does not perform as well when the AIAUV is passively stabilised. This can especially be seen in the slower convergence of the cross-track error in the z-direction in Fig. 2. In this case, not only the joints but also the AIAUV as a whole is influenced by hydrostatic restoring forces which will rotate it, and which are not taken into account in the attitude control method. In contrast, the control law (9) cancels all of the dynamics which influence the reduced attitude in order to achieve tracking of the reference.

5. CONCLUSIONS

In this paper, a control law for reduced attitude tracking was first developed for a general type of system with two control torques, and shown to give asymptotic tracking. A method for controlling the pointing direction of an AIAUV by curving its body was then proposed, using the previously developed control law to provide references for the joints of the AIAUV. The method was used to follow a reference guiding the AIAUV onto and along a straight path, and the applicability of the complete path following method was demonstrated by simulations.

Future topics of interest include deriving the turn dynamics with joint angles as inputs, in order to obtain more precise tracking of the desired pointing direction. The method could also be modified to take into account hydrostatic restoring forces or other disturbances, either in the joint references or by using additional thrusters to improve performance at the cost of increased thruster use.

REFERENCES

Antonelli, G. (2018). *Underwater Robots*. Springer International Publishing, 4th edition.

Bernstein, D.S. (2009). *Matrix Mathematics: Theory, Facts, and Formulas*. Princeton University Press, 2nd edition.

Borlaug, I.L.G., Gravdahl, J.T., Sverdrup-Thygeson, J., Pettersen, K.Y., and Loria, A. (2018a). Trajectory tracking for underwater swimming manipulators using a super twisting algorithm. *Asian J. Control*, 21(1), 208–223.

Borlaug, I.L.G., Pettersen, K.Y., and Gravdahl, J.T. (2018b). Trajectory tracking for an articulated intervention AUV using a super-twisting algorithm in 6 DOF. In *Proc. 11th IFAC Conf. Control Applications in Marine Systems, Robotics, and Vehicles*. Opatija, Croatia.

Bullo, F., Murray, R., and Sarti, A. (1995). Control on the sphere and reduced attitude stabilization. *IFAC Proceedings Volumes*, 28(14), 495 – 501. 3rd IFAC Symp. Nonlinear Control Systems Design.

Caharija, W., Pettersen, K.Y., Gravdahl, J.T., and Sørensen, A.J. (2012). Topics on current compensation for path following applications of underactuated underwater vehicles. *IFAC Proceedings Volumes*, 45(5), 184 – 191. 3rd IFAC Workshop on Navigation, Guidance and Control of Underwater Vehicles.

Chaturvedi, N.A., Sanyal, A.K., and McClamroch, N.H. (2011). Rigid-body attitude control. *IEEE Control Systems*, 31(3), 30–51.

Egeland, O. and Gravdahl, J.T. (2002). *Modeling and Simulation for Automatic Control*. Marine Cybernetics.

Fossen, T.I. (2011). *Handbook of Marine Craft Hydrodynamics and Motion Control*. John Wiley & Sons.

From, P.J., Gravdahl, J.T., and Pettersen, K.Y. (2014). *Vehicle-Manipulator Systems: Modeling for Simulation, Analysis and Control*. Springer-Verlag.

Guo, J. (2006). A waypoint-tracking controller for a biomimetic autonomous underwater vehicle. *Ocean Engineering*, 33(17), 2369 – 2380.

Kelasidi, E., Liljeback, P., Pettersen, K.Y., and Gravdahl, J.T. (2016). Innovation in underwater robots: Biologically inspired swimming snake robots. *IEEE Robotics & Automation Magazine*, 23(1), 44–62.

Khalil, H.K. (2002). *Nonlinear Systems*. Prentice Hall, 3rd edition.

Kohl, A.M., Kelasidi, E., Mohammadi, A., Maggiore, M., and Pettersen, K.Y. (2016). Planar maneuvering control of underwater snake robots using virtual holonomic constraints. *Bioinspiration & Biomimetics*, 11(6).

Lapierre, L. and Jouvencel, B. (2005). Path following control for an eel-like robot. In *Proc. Europe Oceans 2005*, volume 1, 460–465. Brest, France.

Paliotta, C. and Pettersen, K.Y. (2016). Geometric path following with ocean current estimation for ASVs and AUVs. In *Proc. 2016 American Control Conf.*, 7261–7268. Boston, USA.

Piñeirua, M., Godoy-Diana, R., and Thiria, B. (2015). Resistive thrust production can be as crucial as added mass mechanisms for inertial undulatory swimmers. *Phys. Rev. E*, 92.

Pong, C.M. and Miller, D.W. (2015). Reduced-attitude boresight guidance and control on spacecraft for pointing, tracking and searching. *J. Guid. Control Dyn.*, 38(6), 1027–1035.

Ramp, M. and Papadopoulos, E. (2015). Attitude and angular velocity tracking for a rigid body using geometric methods on the two-sphere. In *Proc. 2015 European Control Conf.*, 3238–3243. Linz, Austria.

Sans-Muntadas, A., Kelasidi, E., Pettersen, K.Y., and Brekke, E. (2017). Spiral path planning for docking of underactuated vehicles with limited FOV. In *Proc. 1st IEEE Conf. Control Technology and Applications*. Kohala Coast, Hawaii.

Schmidt-Didlaukies, H., Pettersen, K.Y., and Sørensen, A.J. (2018). Modeling of articulated underwater robots for simulation and control. In *Proc. 2018 IEEE/OES Autonomous Underwater Vehicles*. Porto, Portugal.

Sverdrup-Thygeson, J., Kelasidi, E., Pettersen, K.Y., and Gravdahl, J.T. (2016). Modeling of underwater swimming manipulators. In *Proc. 10th IFAC Conf. Control Applications in Marine Systems*. Trondheim, Norway.

Sverdrup-Thygeson, J., Kelasidi, E., Pettersen, K.Y., and Gravdahl, J.T. (2018). The underwater swimming manipulator - a bioinspired solution for subsea operations. *IEEE J. Oceanic Engineering*, 43(2), 402–417.

Woolsey, C.A. (2006). Directional control of a slender, underactuated AUV using potential shaping. In *Proc. 45th IEEE Conf. Decision and Control*, 6826–6831. San Diego, USA.